

Article

Robust Magnetic γ -Fe₂O₃/Al-ZnO Adsorbent for Chlorpyrifos Removal in Water

Miryam Boulares^{1,2}, Baha Chamam¹, Amal Mejri¹, Mohamed Ali Wahab¹, Amani Haddouk^{1,2}, Lassaad El Mir³, Ahmed Hichem Hamzaoui⁴, Amjad Kallel⁵ , Chedly Tizaoui^{6,*}  and Ismail Trabelsi^{1,*}

- ¹ Laboratory of Treatment and Valorization of Water Reject, Water Research and Technologies Center, Borj-Cedria Technopark, University of Carthage, Soliman 8020, Tunisia; boulares.miryam602@gmail.com (M.B.); baha.chamam@gmail.com (B.C.); mejriamal989@gmail.com (A.M.); waheb_med@yahoo.fr (M.A.W.); amani.haddouk92@gmail.com (A.H.)
- ² Faculty of Sciences of Bizerte, University of Carthage, Jarzouna-Bizerte 7021, Tunisia
- ³ Laboratory of Physics of Materials and Nanomaterials Applied for the Environment (LaPhyMNE), Faculty of Sciences of Gabes, Gabes University, Gabes 6072, Tunisia; lassaad.elmir@fsg.rnu.tn
- ⁴ Laboratory of Materials Valorisation, National Research Centre in Materials Science, Borj-Cedria Technopark, Soliman 8027, Tunisia; mdmih10@gmail.com
- ⁵ Laboratory of Water, Energy and Environment, Sfax National School of Engineering, University of Sfax, Sfax 3038, Tunisia; amjad.kallel@enis.tn
- ⁶ Department of Chemical Engineering, Faculty of Science and Engineering, Swansea University, Swansea SA1 8EN, UK
- * Correspondence: c.tizaoui@swansea.ac.uk (C.T.); ismail.trabelsi@certe.nrnt.tn (I.T.)



Citation: Boulares, M.; Chamam, B.; Mejri, A.; Wahab, M.A.; Haddouk, A.; El Mir, L.; Hamzaoui, A.H.; Kallel, A.; Tizaoui, C.; Trabelsi, I. Robust Magnetic γ -Fe₂O₃/Al-ZnO Adsorbent for Chlorpyrifos Removal in Water. *Water* **2022**, *14*, 1160. <https://doi.org/10.3390/w14071160>

Academic Editor: Alexandre T. Paulino

Received: 14 February 2022

Accepted: 29 March 2022

Published: 4 April 2022

Publisher's Note: MDPI stays neutral with regard to jurisdictional claims in published maps and institutional affiliations.



Copyright: © 2022 by the authors. Licensee MDPI, Basel, Switzerland. This article is an open access article distributed under the terms and conditions of the Creative Commons Attribution (CC BY) license (<https://creativecommons.org/licenses/by/4.0/>).

Abstract: In this research, the removal of the pesticide chlorpyrifos (CPE) from water by adsorption using a novel adsorbent made of γ -Fe₂O₃/Al-ZnO nanocomposite was studied. The adsorbent was characterized using Fourier-transformed infrared spectroscopy (FTIR), Scanning electron microscopy (SEM), Brunauer-Emmett-Teller (BET) surface area, and vibrating sample magnetometry (VSM). The main parameters affecting the adsorption process, including the initial pH (2–12), the concentration of pesticide (10–70 ppm), the %Fe₂O₃ of the adsorbent, and the adsorption time (≤ 60 min), were studied. The results demonstrated that the adsorption of CPE depended on the pH, with a maximum removal of 92.3% achieved at around neutral pH. The adsorption isotherm was modelled and the results showed that the Freundlich model fitted the experimental data better than the Langmuir and Temkin models. The kinetics of adsorption were also studied and modelled using the pseudo-first-order and pseudo-second-order models, with the former being found more suitable. Energy dispersive X-ray (EDX) analysis confirmed the adsorption of CPE on γ -Fe₂O₃/Al-ZnO, while FTIR analysis suggested that the hydroxyl, N-pyridine, and chloro functional groups governed the adsorption mechanism. Furthermore, VSM analysis revealed that the magnetization saturation of γ -Fe₂O₃/Al-ZnO nanocomposite, after CPE adsorption, was slightly lower than that of fresh γ -Fe₂O₃/Al-ZnO but remained adequate for the efficient separation of the adsorbent simply using a magnet. This study demonstrates that binary γ -Fe₂O₃/Al-ZnO magnetic nanocomposites are effective for the removal of chlorpyrifos and could be highly promising materials for the removal of emerging pollutants in wastewater.

Keywords: nanocomposites; magnetic adsorption; chlorpyrifos; pesticides; isotherm and kinetic

1. Introduction

Chlorpyrifos (CPE) (*O,O*-diethyl-*O*-(3,5,6-trichloropyridin-2-yl) phosphorothioate) is one of the most effective organophosphate insecticides used in agriculture and for controlling household pests [1,2]. It was introduced in 1965 as an alternative insecticide to dichlorodiphenyltrichloroethane (DDT) and has since been used widely in at least one hundred countries across the world [1]. However, due to concerns related to its toxicity, CPE was banned from being sold in the European Union in January 2020 [3] and is classified

as a hazardous substance under the Federal Water Pollution Control Act in the USA. CPE is listed as hazardous to humans due to its residual presence in soil, aquifers, and plants and its serious health consequences such as carcinogenicity and inhibition of the enzyme acetylcholine esterase (a key enzyme necessary for nerve function) [4,5]. In addition, CPE acts as an endocrine disruptor with a high potential for binding to androgen receptors, interfering in natural hormonal binding and thus modifying the normal functioning of the endocrine system [6]. Although the use of CPE in the EU and USA is decreasing, it is still widely used in other parts of the world. In Tunisia, CPE is classified as a highly hazardous pesticide, meaning that it presents high levels of acute or chronic hazards to health or the environment, as accepted by international classification systems such as of the World Health Organization (WHO) or Global Health Security (GHS) or their listings in relevant binding international agreements or conventions [7].

The widespread use of CPE has led to the contamination of surface and ground waters [8]. CPE is also present in Wastewater Treatment Plant effluents (WWTPs) [9], with a quantification frequency of <30% in the influents of 15 biological WWTPs at concentrations ranging from 0.1 to 1 $\mu\text{g/L}$ and from 0.01 to 0.1 $\mu\text{g/L}$ in the effluents [10]. Thus, the removal of CPE from the aqueous environment is very important. Several water treatment processes, including solar photo-Fenton [11,12], ozonation [13,14], and adsorption [15,16], have been used to remove pesticides from water. Despite being effective, economical, and routinely used in water treatment [17,18], adsorption has only been seldom studied with regard to the removal of CPE. Voorhees et al. [19] recently evaluated the removal of CPE using granular activated carbon and biochar and demonstrated that both adsorbents were effective to reduce CPE to less than detectable and non-toxic concentrations. Diatomaceous earth was also tested and was found to remove 95% of chlorpyrifos from river and waste waters [20]. In a mixture of seven different pesticides (alachlor, metolachlor, chlorpyrifos, fipronil, α -endosulfan, β -endosulfan, and *p,p'*-DDT), fixed-bed adsorption, using rice husk ash (RHA) as an adsorbent, was also found to be effective for the removal of CPE. The column elution studies showed that 10 L of the mixed pesticide-contaminated water (0.05 mg/L) could be treated with only 10 g of RHA at a removal efficiency of 90% [21]. The use of nanoscale *Moringa oleifera* seed waste (nMSW) as a nano-biosorbent was also tested for CPE removal from contaminated wastewater, achieving an 81% removal at pH 7 and a 30 min adsorption contact time [16].

Although activated carbon is an adsorbent that is widely used for the removal of pesticides in water, it has several drawbacks, including its high regeneration costs and brittle nature. There are also concerns about the environmental footprint of the current methods used to produce and regenerate activated carbon [22,23]. Therefore, there has been growing interest in the use of new adsorbents that could be efficiently used in wastewater treatment. In our previous study [24], $\gamma\text{-Fe}_2\text{O}_3/\text{Al-ZnO}$, a ferromagnetic binary nanocomposite, was found to present remarkable adsorption properties, making it an excellent material for fabricating gas-phase acetone sensors. In the present study, we explore, for the first time, the use of this material as a novel nanocomposite adsorbent for the treatment of wastewater contaminated with chlorpyrifos pesticide. The $\gamma\text{-Fe}_2\text{O}_3/\text{Al-ZnO}$ nano-adsorbent synthesized in this study was characterized using the Fourier Transform Infrared Spectroscopy (FTIR), scanning electron microscopy (SEM), energy-dispersive X-ray spectroscopy (EDX), and vibrating sample magnetometer (VSM) techniques before and after the adsorption of CPE. The effects of the variables pH, initial CPE concentration, and adsorption contact time were evaluated. The adsorption isotherms and kinetics were also determined and analyzed using appropriate adsorption models. This study presents, for the first time, the application of magnetic nanocomposite $\gamma\text{-Fe}_2\text{O}_3/\text{Al-ZnO}$ as an adsorbent to remove the pesticide chlorpyrifos from water.

2. Materials and Methods

2.1. Reagents

High Performance Liquid Chromatography (HPLC) grade acetonitrile and methanol were purchased from Advent Chembio PVT Ltd., India, and high-purity (>98%) analytical-grade chlorpyrifos-ethyl (CPE) was purchased from Sigma Aldrich, USA. ACS reagent-grade hydrochloric acid (HCl) and sodium hydroxide (NaOH) were provided by VWR chemicals, USA. Milli-Q water was generated from a Direct-Q Ultrapure Water System from Heal Force (Bio-Meditech Holdings Group, Shanghai, China) with a specific resistance of 18.2 MΩ.cm and a total organic carbon (TOC) content of 2 µg/L. The experiments were carried out in Milli-Q water as well as in CPE-spiked real secondary-treated wastewater.

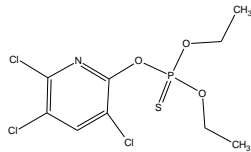
2.2. Real Wastewater

Urban wastewater samples (influent and effluent) were collected from Choutrana II WWTP, located in north Tunisia. The plant operates on activated sludge biological treatment at an average inlet flow of 0.46 m³/s. Wastewater samples were collected from the treatment plant in pre-rinsed amber glass bottles (2 L) and filtrated immediately through a 0.45 µm Membrane Filter (MF-Millipore™, Merck Life Science, Mumbai, India). The samples were then stored at 4 °C in the dark until testing. The effluent from the plant had the following characteristics: pH 7.31 ± 0.1, 5-day Biological Oxygen Demand (BOD₅) 461 ± 94 mg/L, conductivity 2.39 ± 0.2 mS/cm, turbidity 3.59 ± 3.0 NTU, Total Organic Carbon (TOC) 11.3 ± 2.0 mg/L, Inorganic Carbon (IC) 55.4 ± 2.0 mg/L, Cl⁻ 573.3 ± 100.0 mg/L, PO₄³⁻ 29.2 ± 2.8 mg/L, SO₄²⁻ 300.3 ± 50.0 mg/L.

2.3. Preparation and Analysis of Chlorpyrifos Solutions

A stock solution of CPE at 1000 mg/L was prepared in acetonitrile and kept in the fridge at 4 °C. Aqueous working solutions at given concentrations in the range 10 to 70 mg/L were prepared by diluting the stock solution with Milli-Q water. The aqueous solution pH was adjusted with hydrochloric acid (HCl) and sodium hydroxide (NaOH) at concentrations of 0.01 M each. Table 1 gives the selected physico-chemical properties of CPE. The concentration of CPE in water was determined by a UV/Vis spectrophotometer (Perkin ELMER Lambda 25 UV/Vis Spectrophotometer, Loyola Marymount University, Los Angeles, CA, USA) using a pre-determined calibration curve at the maximum absorbance wavelength λ_{max} = 289 nm; λ_{max} was determined by measuring the UV/Vis spectrum of a 50 mg/L CPE solution in the wavelength range of 200 to 850 nm, and its value of 289 nm agreed well with the literature [25,26]. Eight CPE concentrations in the range of 10 to 80 mg/L were used to determine the calibration curve.

Table 1. Physical/chemical properties of chlorpyrifos (CPE).

Properties	Chlorpyrifos	References
Chemical name: <i>O,O</i> -diethyl- <i>O</i> -(3,5,6-trichloropyridin-2-yl) phosphorothioate	C ₉ H ₁₁ NO ₃ PSCl ₃	
Chemical formula		[27]
Physical description	White crystalline solid	
Molecular mass	350.6 g/mol	
Water solubility	1.4–2 mg/L at 25 °C	
Partitioning coefficient (Log K _{ow})	4.96–5.11	[28]

2.4. Synthesis and Characterization of γ -Fe₂O₃/Al-ZnO Adsorbent

The synthesis of γ -Fe₂O₃/Al-ZnO was carried out using a two-step method [24]. In the first step, 8 g of zinc acetate dehydrate (Zn (CH₃COO)₂ × 2H₂O, >99%, Sigma-Aldrich, St. Louis, MO, USA) was dissolved in 56 mL of methanol (CH₃OH, 99.8%, Sigma-Aldrich, St. Louis, MO, USA). After 15 min of magnetic stirring at room temperature, an adequate quantity of aluminum nitrate-9- hydrate (Al(NO₃)₃ × 9H₂O, >99%, Sigma-Aldrich, St. Louis, MO, USA) was added to obtain an Al/Zn ratio of 0.03, where Al was the doping element. After 20 min of stirring using a magnetic stirrer, 280 mL of ethanol absolute (CH₃CH₂OH, >99.9%, Sigma-Aldrich, St. Louis, MO, USA) was added and the solution was dried in an autoclave under supercritical conditions of ethanol (T_c = 243 °C; P_c = 63.6 bar) to produce Al-ZnO nanoparticles. In the second step, 16 g of iron (III) precursor (acetylacetonate) (C₁₅H₂₁FeO₆, >99.9%, Sigma-Aldrich, St. Louis, MO, USA) was dissolved in 32 mL of methanol, to which different quantities of Al-ZnO nanoparticles prepared in the first step were added. After stirring for 15 min, 220 mL of ethanol was added, and the solution was dried in an autoclave at the supercritical conditions of ethanol similarly to the first step to finally obtain γ -Fe₂O₃/Al-ZnO nanocomposite [24].

The prepared γ -Fe₂O₃/Al-ZnO nanocomposite adsorbent at a loading of 24.52% γ -Fe₂O₃ was characterized before and after the removal of chlorpyrifos using various techniques. The adsorbent prepared at this γ -Fe₂O₃ loading was selected for characterization because of its highest removal rate of CPE in comparison to the other adsorbents, as determined by the adsorption study. The adsorbent functional groups were characterized by Fourier-transform infrared (FTIR) spectroscopy (IR Affinity-1 SHIMADZU FT-IR Spectrometer, Kyoto, Japan) using transmittance spectra in the range of 4000 to 100 cm⁻¹ in KBr pellets. The adsorbent morphology and structure were observed using a Quattro ESEM Thermo-Fisher, UK, in combination with Energy-Dispersive X-ray (EDX, MODEL JSM-IT200) operated at 5–15 kV. Brunauer–Emmett–Teller (BET) surface area and pore size measurements were also conducted at 77 K using N₂ adsorption/desorption isotherms (Nova 200e, Quantachrome Instruments, Boynton Beach, FL, USA). The samples were degassed at 150 °C for 4 h before nitrogen adsorption measurements. The Quantachrome NovaWin package was used for data acquisition and analysis. The point of zero charge (PZC) of the adsorbent was also determined in this study by plotting the zeta potential values against pH; the pH that gave zero zeta potential was denoted the PZC. The zeta potential was calculated from the electrophoretic mobility of γ -Fe₂O₃/Al-ZnO at 25 ± 0.1 °C in a capillary cell (ZET 5104) of the Zetasizer 4 (Malvern, UK) apparatus. Measurements of the electrophoretic mobility were converted to zeta potentials based on Smoluchowski approximation (k.a >> 1). Before measurement, a given amount of the adsorbent (20 mg) was added to 100 mL of distilled water. Six samples were prepared in the same manner and the pH of each sample was adjusted using 0.1 mol/L HCl and 0.1 mol/L NaOH solutions. Magnetization curves of the synthesized nanocomposite were also measured using a vibrating sample magnetometer VSM 4500 (EG & G Princeton applied Research, City, Oak Ridge, TN, USA) at ambient temperature.

2.5. Batch Adsorption Experiments

Experiments on CPE sorption onto γ -Fe₂O₃/Al-ZnO in aqueous media were performed in batch mode. A volume of 5 mL of sample was used for the adsorption experiments. The pH was adjusted by the addition of HCl (0.01 M) or NaOH (0.01 M) and measured by a pH meter (Consort C831). A fixed dosage of adsorbent of 0.5 g/L was used in all experiments and the contact time was set to 60 min, while the adsorption temperature was set to 22 ± 2 °C in all experiments. The adsorbent uptake of CPE was determined from the mass balance shown in Equation (1), and the removal efficiency of CPE (%) was calculated using Equation (2). In addition, experiments on adsorbent reuse were conducted after adsorption, followed by seven repeated washes of the adsorbent with hot water at 40 °C.

$$q = \frac{V(C_0 - C)}{m} \quad (1)$$

$$R(\%) = 100 \times \frac{C_0 - C}{C_0} \tag{2}$$

where q is the adsorbent uptake (mg/g); V is the solution volume (L); C_0 and C are the initial and after-adsorption concentrations, respectively (mg/L); m is the mass of the adsorbent (g); and $R(\%)$ is the removal efficiency (%).

2.6. Data Analysis

2.6.1. Adsorption Kinetics Models

The rate of adsorption of CPE was determined using the pseudo-first-order (PFO) and pseudo-second-order (PSO) models. These models expressed in linear forms are shown by Equations (3) and (4) for PFO and PSO, respectively:

$$\ln\left(\frac{q_e - q_t}{q_e}\right) = -k_1 t \tag{3}$$

$$\frac{t}{q_t} = \frac{1}{k_2 q_e^2} + \frac{t}{q_e} \tag{4}$$

where q_e and q_t (mg/g) are the CPE uptake at equilibrium and at a time t , respectively; k_1 (min^{-1}) is the pseudo-first-order rate constant; and k_2 ($\text{g}/(\text{mg}\cdot\text{min})$) is the pseudo-second-order rate constant.

2.6.2. Isotherms of CPE Adsorption on $\gamma\text{-Fe}_2\text{O}_3/\text{Al-ZnO}$

Adsorption isotherms are very important in adsorption studies to optimize the adsorption process and develop an understanding of the sorbate/sorbent interactions. Experimental isotherm data were fitted using three two-parameter sorption isotherms commonly used in adsorption studies, including the Freundlich, Langmuir, and Temkin models. The equations for each model, represented in linear form, are shown in Table 2 [29,30], and the parameters of each model were determined from the slope and intercept of the linear plots, as shown in Table 2. The experiments were repeated at least twice and the average errors varied between 3 and 8%.

Table 2. Isotherm equations for the adsorption of CPE on $\gamma\text{-Fe}_2\text{O}_3/\text{Al-ZnO}$.

Model	Linear Form	Plot	Parameters
Langmuir	$\frac{C_e}{q_e} = \frac{1}{K_L q_m} + \frac{C_e}{q_m}$	$\frac{C_e}{q_e}$ vs. C_e	$q_m = \frac{1}{\text{slope}}$; $K_L = \frac{\text{slope}}{\text{intercept}}$
Freundlich	$\ln(q_e) = \ln(K_f) + \frac{1}{n} \ln(C_e)$	$\ln(q_e)$ vs. $\ln(C_e)$	$K_f = \exp(\text{intercept})$; $\frac{1}{n} = \text{slope}$
Temkin	$q_e = \frac{RT}{b_T} \ln(a_T) + \frac{RT}{b_T} \ln(C_e)$	q_e vs. $\ln(C_e)$	$a_T = \exp\left(\frac{\text{intercept}}{\text{slope}}\right)$; $b_T = \frac{RT}{\text{slope}}$

C_e is the equilibrium CPE concentration in solution (mg/L); q_m is the maximum adsorption capacity corresponding to complete monolayer coverage of the surface (mg/g) and K_L is the Langmuir adsorption constant (L/mg); K_f and $1/n$ are characteristic constants representing the adsorption capacity and intensity, respectively; a_T is the Temkin isotherm constant, b_T is the Temkin constant related to heat of sorption (kJ/mol), R is the ideal gas constant (8.314 J/(mol.K)), and T is the absolute temperature (K).

3. Results

3.1. Characterization of $\gamma\text{-Fe}_2\text{O}_3/\text{Al-ZnO}$ Adsorbent

3.1.1. SEM and EDX Analyses of $\gamma\text{-Fe}_2\text{O}_3/\text{Al-ZnO}$

Morphological and elemental analyses at the adsorbent surface before (Figure 1A,B) and after (Figure 1C,D) CPE adsorption were conducted using SEM/EDX. The SEM images show the porous structure of the synthesized adsorbent, which is typical for $\gamma\text{-Fe}_2\text{O}_3/\text{Al-ZnO}$ nanocomposites [24]. This porous structure is favorable for the adsorption of molecules

and has been exploited in other studies to develop gas sensors. According to the results obtained from the EDX analysis, the mass percentages ($w/w\%$) of the elements before and after CPE adsorption are shown in Table 3. A strong signal of iron was observed in fresh $\gamma\text{-Fe}_2\text{O}_3/\text{Al-ZnO}$ (Figure 1B), indicating that the surface is densely covered by iron, which is in agreement with the findings of other studies [31,32]. As shown in Table 3, the mass percentages of the elements C, N, P, S, and Cl increased from non-detectable values before CPE adsorption to 3.08, 0.24, 0.26, 0.25, and 0.34%, respectively, after CPE adsorption, providing evidence that CPE was effectively adsorbed on the surface of $\gamma\text{-Fe}_2\text{O}_3/\text{Al-ZnO}$.

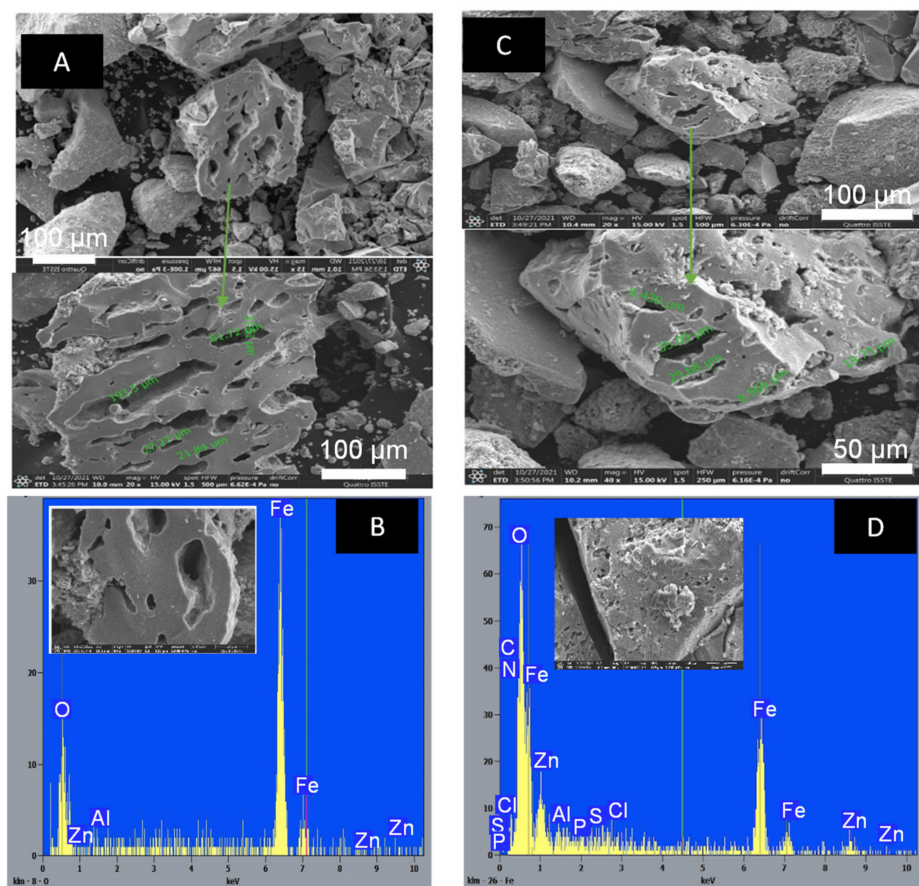


Figure 1. (A) SEM images and (B) EDX of $\gamma\text{-Fe}_2\text{O}_3/\text{Al-ZnO}$ before chlorpyrifos adsorption; (C) SEM images and (D) EDX of $\gamma\text{-Fe}_2\text{O}_3/\text{Al-ZnO}$ after chlorpyrifos adsorption.

Table 3. Quantitative results of EDX.

Element	Before Adsorption		After Adsorption of CPE	
	% Mass	% Atomic	% Mass	% Atomic
O	9.05	25.73	27.93	53.86
Al	0.30	0.51	0.42	0.48
Fe	90.04	73.34	56.78	31.37
Zn	0.61	0.42	10.70	5.05
C	n.d *	n.d	3.08	7.92
N	n.d	n.d	0.24	0.53
P	n.d	n.d	0.26	0.26
S	n.d	n.d	0.25	0.24
Cl	n.d	n.d	0.34	0.29

n.d *: not detected.

3.1.2. FTIR Analysis of Fe₂O₃/Al-Zn before and after CPE Adsorption

According to Figure 2A, the main changes in the IR spectra before and after the adsorption of chlorpyrifos were observed at 3500, 1630, 1393, 1112, and 963 cm⁻¹ peaks. The broad peaks centered at the bands 3450–3500 and 1630–1640 cm⁻¹ can be assigned to the stretching and bending vibrations of the hydroxyl groups or water molecules, respectively. The peak at around 3450 cm⁻¹ in the CPE spectrum could be due to the C-H bending of the ethoxy groups [33]. After CPE adsorption, band 3450–3500 cm⁻¹ became wider, indicating that hydroxyl groups were involved in the adsorption process [16], possibly through a mechanism involving hydrogen bonding between hydroxyl groups on the surface of the adsorbent and the N-pyridine group as well as the terminal Cl atoms, as depicted in Figure 2B [34,35]. Furthermore, shifts in the peak positions at 1407, 1328, 1050, and 750 cm⁻¹, which are characteristic of C=C stretching, C-H stretching, C-O bending, and C-Cl stretching, respectively, were also recorded after CPE adsorption. These shifts in bands to new wave numbers after CPE adsorption provide evidence of interactions between the surface of the adsorbent and CPE. Consequently, the mechanism of CPE adsorption could involve hydrogen bonding, possibly between the terminal hydrogen atoms of the methyl group of CPE and the oxygen atoms present on the adsorbent surface. In addition, the after-adsorption spectrum shows that the C-Cl stretching band (~630 cm⁻¹) became weaker possibly due to the coordination of CPE to γ -Fe₂O₃/Al-ZnO through its Cl atom. This pathway of interaction between CPE and the adsorbent is plausible, given the abundance of the chloro-group in the CPE molecule, and is also in agreement with the results of other studies. For example, using density functional theory, adsorption through the Cl pathway was found to be an important mechanism of the adsorption of 2-chlorophenol from water on γ -Fe₂O₃ [36]. In the IR spectrum of adsorbed CPE, a band appeared at 1393 cm⁻¹ which is characteristic of C-H bending, and peaks at 1059 and 963 cm⁻¹, which correspond to C-O and P-O stretching, respectively, also appeared. The appearance of these bands provides further evidence of CPE adsorption. Accordingly, CPE adsorption on γ -Fe₂O₃/Al-ZnO is feasible and proceeds through interactions involving hydroxyl groups, chlorine atoms, N-pyridine, and hydrogen bonding.

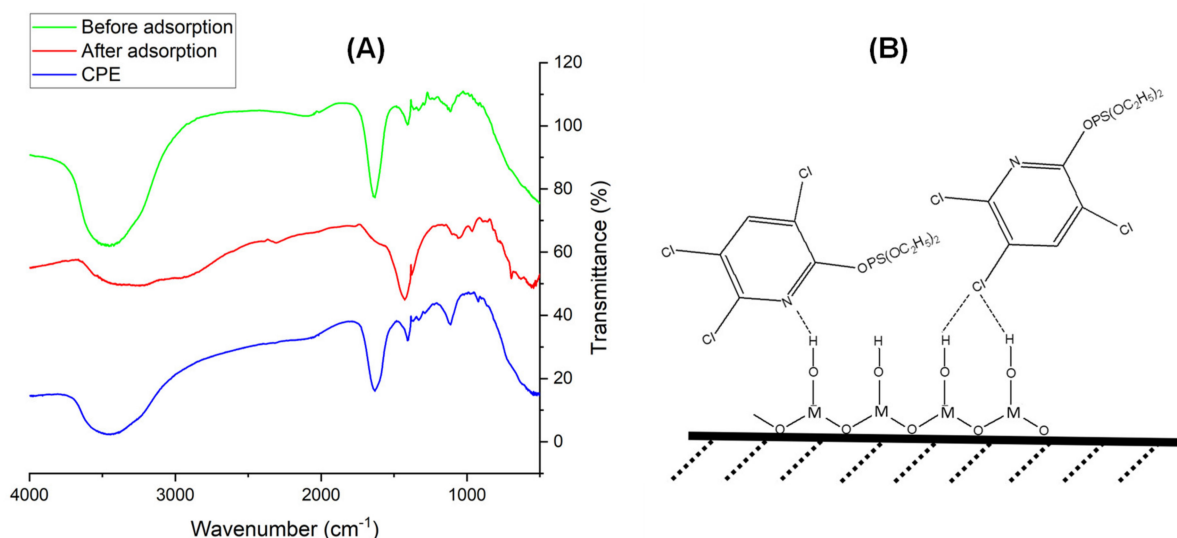


Figure 2. (A) FTIR spectrum before and after CPE adsorption; (B) suggested mechanism for CPE interaction with the adsorbent.

3.1.3. BET Surface Area and Pore Size

The BET surface area of the adsorbent was measured according to the BET equation applied in the range $P/P^{\circ} < 0.3$ (Figure 3A) and its value was found to be equal to 28.14 ± 1.48 m²/g. This BET surface area was comparable to that reported for γ -Fe₂O₃/Al-ZnO [24] and was about three times higher than the surface areas reported for other

Fe_2O_3 -based adsorbents [37]. The pore size distribution was examined using the Dubinin–Astakhov (DA) model, which is suitable for microporous materials. The DA model showed that the average pore size of the adsorbent was 15 Å (Figure 3B), which confirms the microporous nature of the material. The microporous nature and high surface area of the material indicate the strong adsorption capacity of $\gamma\text{-Fe}_2\text{O}_3/\text{Al-ZnO}$, as will be demonstrated in the following sections.

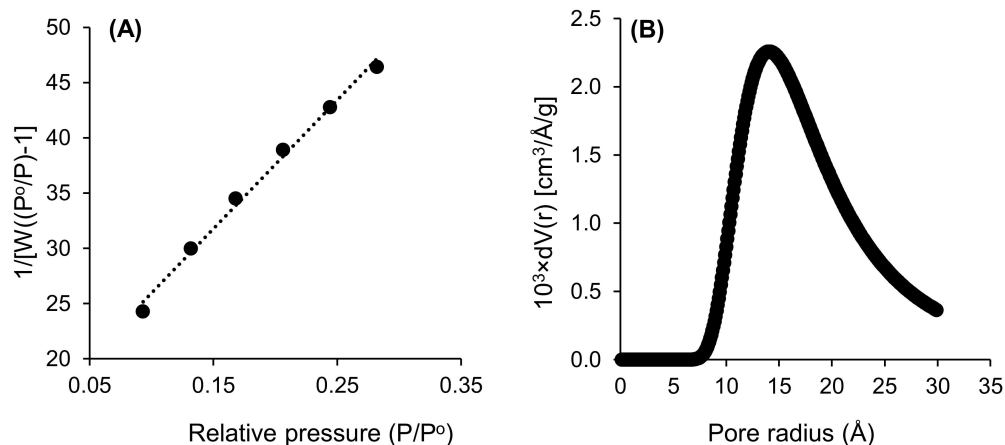


Figure 3. (A) BET plot and (B) Dubinin–Astakhov plot.

3.1.4. Vibrating Sample Magnetometry (VSM)

The magnetization curves of raw $\gamma\text{-Fe}_2\text{O}_3/\text{Al-ZnO}$ and $\gamma\text{-Fe}_2\text{O}_3/\text{Al-ZnO}$ after the adsorption of CPE are shown in Figure 4. The curves show that $\gamma\text{-Fe}_2\text{O}_3/\text{Al-ZnO}$ maintained its magnetic property after being loaded with CPE. According to the shape of the obtained curves, the material has a magnetic memory, with superparamagnetic behavior explained by the absence of hysteresis. The magnetization saturation values determined at 189 K were 37.8 and 29.9 emu/g for $\gamma\text{-Fe}_2\text{O}_3/\text{Al-ZnO}$ before and after CPE adsorption, respectively. Although the adsorption of CPE slightly reduced the magnetization saturation of $\gamma\text{-Fe}_2\text{O}_3/\text{Al-ZnO}$, the adsorbent was recoverable from the aqueous medium by the simple application of an external magnetic field (Figure 4 inset).

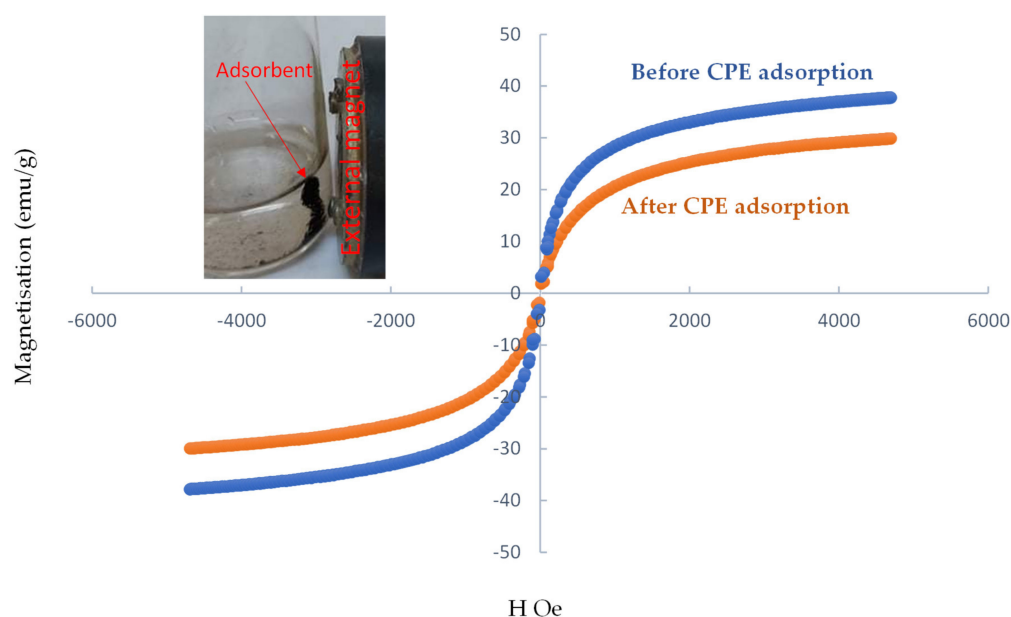


Figure 4. Magnetization hysteresis loop for $\gamma\text{-Fe}_2\text{O}_3/\text{Al-ZnO}$ before and after CPE adsorption.

3.2. Optimization of Parameters Affecting CPE Removal by γ -Fe₂O₃/Al-ZnO

3.2.1. Effect of the Fe₂O₃ Loading on the Adsorbent Removal Efficiency

Five different γ -Fe₂O₃/Al-ZnO adsorbents were prepared at different loadings of γ -Fe₂O₃ (24.52%, 39.39%, 49.36%, 56.52%, and 61.90%). Their CPE adsorption capacities and removal rates versus time were determined using CPE at an initial concentration of 50 mg/L and the adsorbent dose was kept the same at 0.5 g/L. The results presented in Figure 5 indicated that high adsorption capacities were achieved at an equilibrium time of 30 min for the five adsorbents, but the adsorbent doped with 24.52% γ -Fe₂O₃ gave the highest CPE removal (92.33%). The removal of CPE by the other adsorbents after 30 min of contact time were only 91.19, 91.02, 90.96, and 85.80% for γ -Fe₂O₃ loadings of 39.39%, 49.36%, 56.52%, and 61.90%, respectively. According to these results, the percentage of CPE elimination by γ -Fe₂O₃/Al-ZnO is inversely proportional to γ -Fe₂O₃ loading. In a study conducted by Zahmouli et al. [24], a similar γ -Fe₂O₃ loading to that obtained in this study was also found to be the best γ -Fe₂O₃ loading for their acetone-sensing application. The adsorbent prepared with a 24.52% γ -Fe₂O₃ loading was selected for use in the remainder of the study.

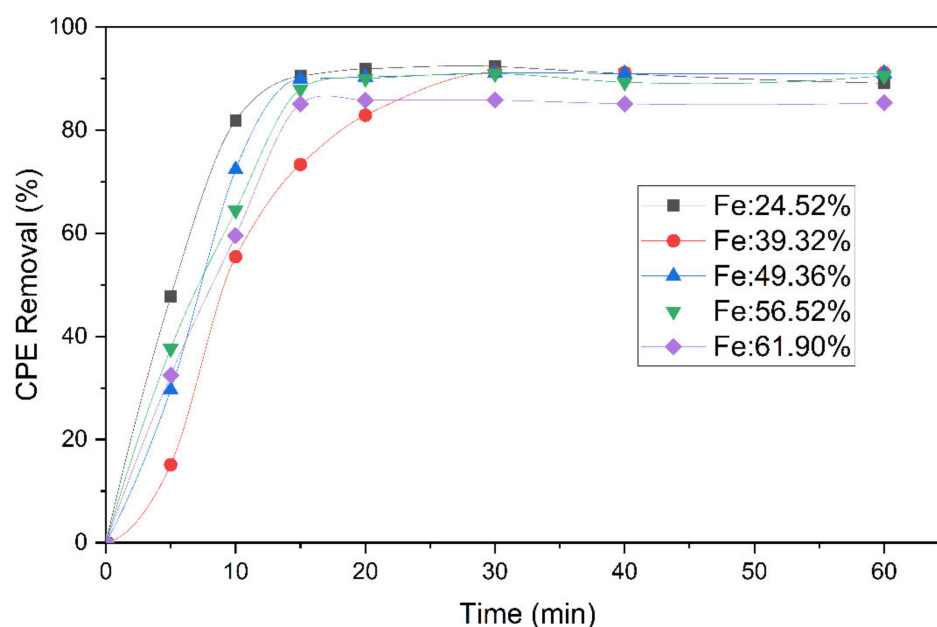


Figure 5. Effect of γ -Fe₂O₃ loading on CPE adsorption (pH = 6.8, C₀ = 50 mg/L, adsorbent dose = 0.5 g/L, and T = 22 ± 2 °C).

3.2.2. Effect of Initial pH

The effect of solution pH on CPE removal using γ -Fe₂O₃/Al-ZnO sorbent was investigated at pH values ranging between 2.0 and 12.0 with an initial CPE concentration of 50 mg/L. As shown in Figure 6A, the CPE removal percentage decreased at higher and lower pH values, giving pH 7 as optimum for the adsorption of CPE on γ -Fe₂O₃/Al-ZnO. The point of zero charge of γ -Fe₂O₃/Al-ZnO was determined in this study and its value was found to be equal to pH 1.1 (Figure 6B). This means that at all the experimental pH values used for adsorption in this study, the surface of the adsorbent is expected to be negatively charged. Thus, at low pH values (pH < 7), the high concentrations of protons (H⁺) in solution strongly competed for the negatively charged sites on the surface of the adsorbent, which led to a strong reduction in CPE adsorption as the pH was below 7, as observed in Figure 6A. At high pH values (pH > 7), the lower removal of CPE might be attributed to the deprotonation and hydrolysis of the functional groups on the surface of the adsorbent, which could diminish the active sites available for hydrogen bonding between CPE and the adsorbent surface, thereby leading to a reduction in adsorption [38].

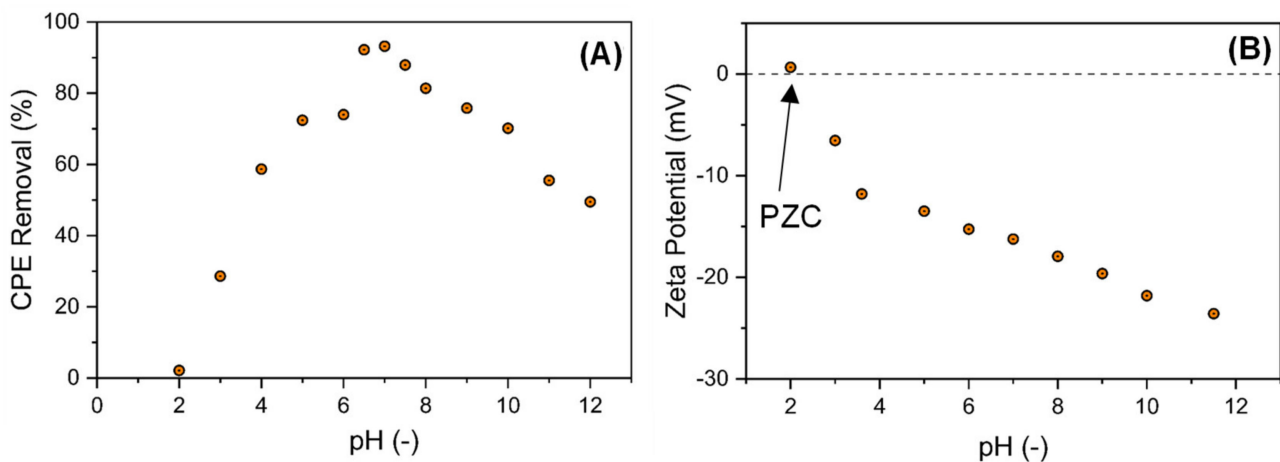


Figure 6. (A) Effect of pH on CPE adsorption onto $\gamma\text{-Fe}_2\text{O}_3/\text{Al-ZnO}$ ($C_0 = 50 \text{ mg/L}$; contact time = 30 min; volume of solution = 5 mL; sorbent dose = 0.5 g/L). (B) PZC of $\gamma\text{-Fe}_2\text{O}_3/\text{Al-ZnO}$.

3.3. Isotherm of CPE Adsorption onto $\gamma\text{-Fe}_2\text{O}_3/\text{Al-ZnO}$

The determination of adsorption equilibrium isotherms is very important for the evaluation of the feasibility of the adsorption process in retaining the sorbate from aqueous media to the solid phase. Consequently, the adsorption isotherm of CPE onto $\gamma\text{-Fe}_2\text{O}_3/\text{Al-ZnO}$ at a 24.52% $\gamma\text{-Fe}_2\text{O}_3$ loading was evaluated at 22 °C using different initial solution concentrations, while the adsorbent dose was kept constant at 0.5 g/L. Three different but commonly used models were used to describe the experimental data: Langmuir, Freundlich, and Temkin (Figure 7).

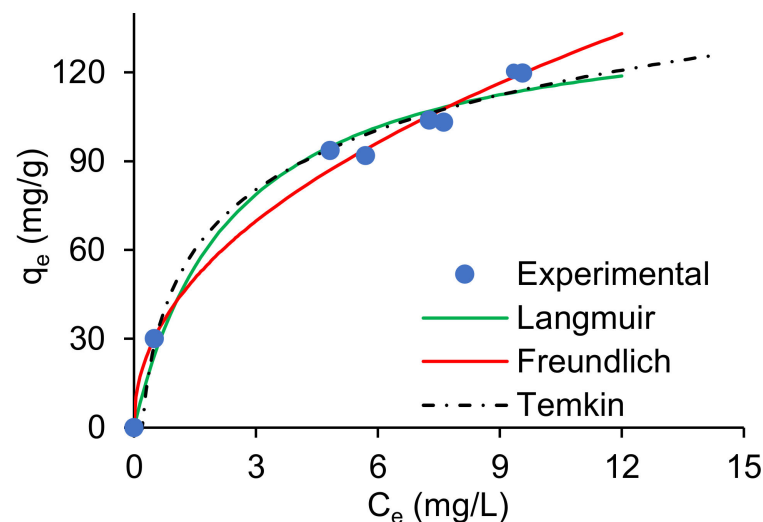


Figure 7. Freundlich, Langmuir, and Temkin isotherms for CPE adsorption onto $\gamma\text{-Fe}_2\text{O}_3/\text{Al-ZnO}$ (pH 6.8; temperature = $22 \pm 2 \text{ }^\circ\text{C}$).

Table 4 summarizes the parameters of each model and the correlation coefficients between the experimental and model results (R^2). Comparing the closeness of the determination coefficients (R^2) to one shows that the CPE adsorption onto $\gamma\text{-Fe}_2\text{O}_3/\text{Al-ZnO}$ follows the Freundlich model slightly better than the Langmuir or Temkin models. The Freundlich model is commonly used to describe adsorption in liquid phases. It could thus be stated that the adsorption of CPE proceeds through heterogeneous multilayer adsorption [39]. A similar isotherm model was also observed for the adsorption of CPE onto the nanoparticles of water treatment residuals [20]. The adsorption of CPE onto $\gamma\text{-Fe}_2\text{O}_3/\text{Al-ZnO}$ was found to be favorable, as demonstrated by the Freundlich equation and supported by the R_L

constant of the Langmuir isotherm being between 0 and 1 under the different initial CPE concentrations (10–75 mg/L) used in this study (Table 4).

Table 4. Isotherm parameters and correlation coefficients calculated for the sorption of CPE onto $\gamma\text{-Fe}_2\text{O}_3/\text{Al-ZnO}$.

Isotherm	Parameter	Value
Freundlich	$K_f (\text{L}^{0.466} \text{mg}^{0.534} \text{g}^{-1})$	41.79
	$1/n$	0.4660
	R^2	0.9989
Langmuir	$K_L (\text{L}/\text{mg})$	0.409
	$q_m (\text{mg}/\text{g})$	142.86
	RL	0.034–0.047
	R^2	0.9968
Temkin	a_T	5.254
	$b_T (\text{kJ}/\text{mol})$	84.21
	R^2	0.9977

3.4. Adsorption Kinetics

The effect of the initial CPE concentration on the kinetics of adsorption (i.e., the rate of approach to equilibrium) was investigated using CPE concentrations in the range of 10 to 70 mg/L, while the dose of the adsorbent was kept constant at 0.5 g/L. Figure 8 (only initial concentrations of 50 and 70 mg/L are presented for clarity) shows the change in CPE uptake by $\gamma\text{-Fe}_2\text{O}_3/\text{Al-ZnO}$ as a function of time. The figure clearly indicates that the adsorption process was rapid, with equilibrium being reached in about 20 min or less. The rapid adsorption rate observed at the beginning can be explained by a strong affinity between the adsorbent surface and CPE, as also demonstrated by the high value of the Freundlich constant, K_F , and the high interaction between CPE and the adsorbent shown by the FTIR analysis. In addition, the rapid adsorption rate supports the suggested mechanism of adsorption via the chloro pathway, which was demonstrated in other studies to be a fast pathway [36]. The equilibrium uptake concentration (q_e) increased when the initial solution concentration increased. This increase in q_e was expected, since adsorption is a phase equilibrium operation, which means that, fundamentally, the uptake by the solid phase increases with the solute concentration in solution. To model the adsorption kinetics, two kinetic equations were used to fit the experimental data, including the pseudo-first-order (PFO) and the pseudo-second-order (PSO) kinetic models (Equations (3) and (4)). The values of the average R^2 , relative to initial concentrations, were $0.974 \pm 1\%$ and $0.948 \pm 2\%$ for the pseudo-first-order and pseudo-second-order models. Thus, the pseudo-first-order model was deemed to be more appropriate for describing the kinetics of CPE adsorption on $\gamma\text{-Fe}_2\text{O}_3/\text{Al-ZnO}$. The average pseudo-first-order rate constant, k_1 , was found to be equal to $0.190 \pm 13\% \text{ min}^{-1}$. In their study on the adsorption of CPE on drinking water treatment residues, Hamadeen et al. also demonstrated that CPE adsorption was described by a pseudo-first-order model but with a rate constant that was much lower (0.0077 min^{-1}) than that obtained in our study [40].

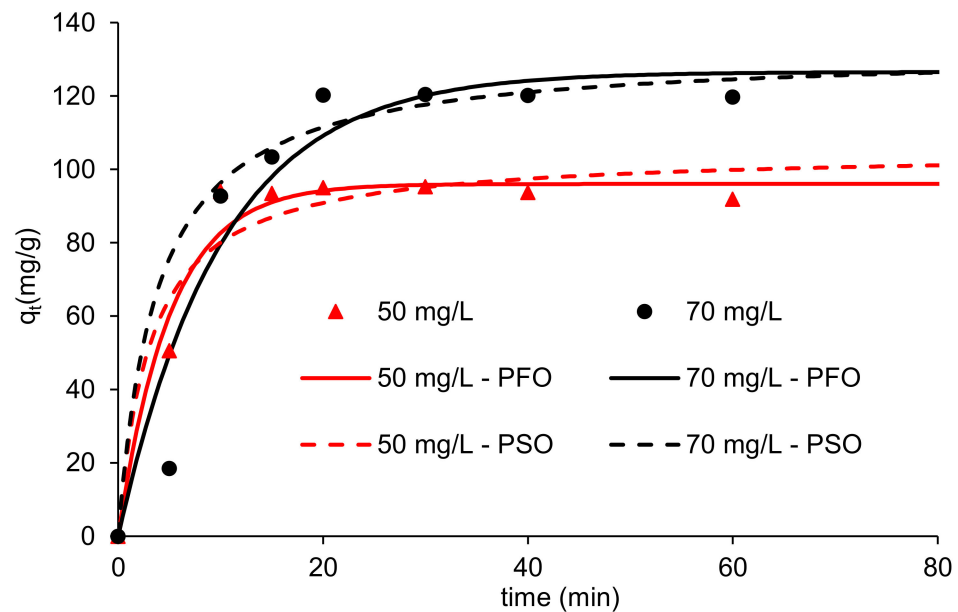


Figure 8. Kinetics of CPE adsorption on $\gamma\text{-Fe}_2\text{O}_3/\text{Al-ZnO}$ (sorbent dose 0.5 g/L, initial solution pH 6.8, temperature = 22 ± 2 °C).

3.5. Reuse of the Adsorbent and Application in Real Wastewater

The reuse of the adsorbent was investigated through repeated adsorption–desorption cycles. The regeneration of the adsorbent between cycles was achieved by seven successive washings (i.e., desorption) with hot water at 40 °C. The cumulative recovery of CPE in water during the desorption experiment is shown in Figure 9A. The figure shows that after about five washings, about 99% of the initially adsorbed CPE mass was recovered in wash water. A further two washings were performed to ensure the complete regeneration of the adsorbent. CPE adsorption was performed for 30 min and the change in CPE concentration in water was used to calculate the removal percentage. As shown in Figure 9B, the removal percentage was reduced from about 92% to about 80% after the second use to a removal percentage of about 63% after the third use, which remained constant for the further adsorption/desorption cycles. Despite this observed reduction in removal after reuse, which was due to a modest increase in experimental temperature ~ 30 °C, the adsorbent remained active towards CPE adsorption.

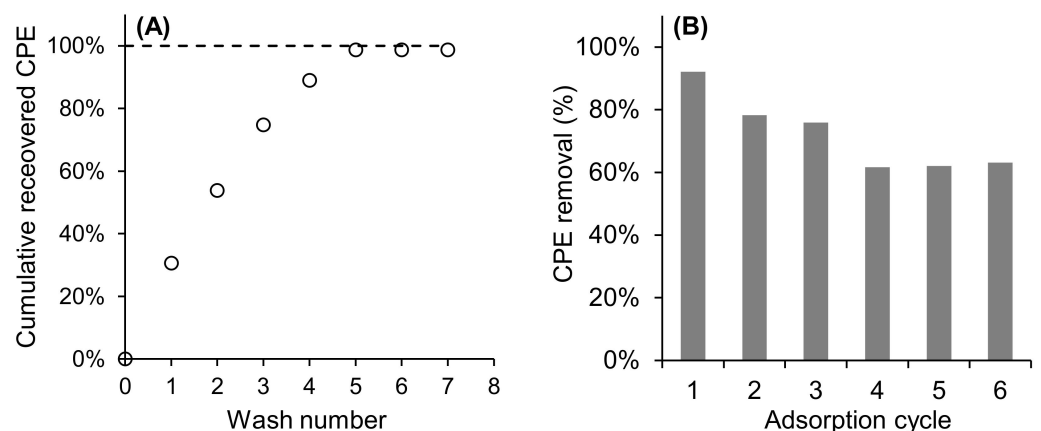


Figure 9. Adsorbent re-use: (A) effect of washing cycles on CPE recovery and (B) effect of reuse cycles on CPE adsorption.

To evaluate the performance of $\gamma\text{-Fe}_2\text{O}_3/\text{Al-ZnO}$ in real wastewater, adsorption experiments were conducted using secondary-treated wastewater from the Choutrana WWTP

spiked with CPE at 50 mg/L. The experimental conditions were kept the same as those in the study with Milli-Q water, including an ambient temperature of 22 °C, pH = 6.8, and adsorbent dose of 0.5g/L. As shown in Figure 10, the kinetics of CPE adsorption in the wastewater were rapid at the beginning of the adsorption process and reached a plateau after about 20 min in a similar profile as that used in the CPE adsorption in Milli-Q water. The pseudo-first-order equation was used to model the adsorption kinetics in both Milli-Q water and real wastewater. The values of the PFO rate constant, k_1 , were 0.191 min⁻¹ and 0.157 min⁻¹ for Milli-Q water and real wastewater, respectively, indicating that the adsorption rate in real wastewater was slightly slower than the rate in Milli-Q water. In addition, an appreciable reduction in the equilibrium uptake amounting to about 15% between Milli-Q water and real wastewater was observed (Figure 10). This reduction in equilibrium uptake could be due to competition for adsorption sites with other molecules and ions contained in wastewater. Other studies have also shown that the adsorption uptake in real wastewaters, which are inherently complex matrices, reduces in comparison to that in distilled water [40].

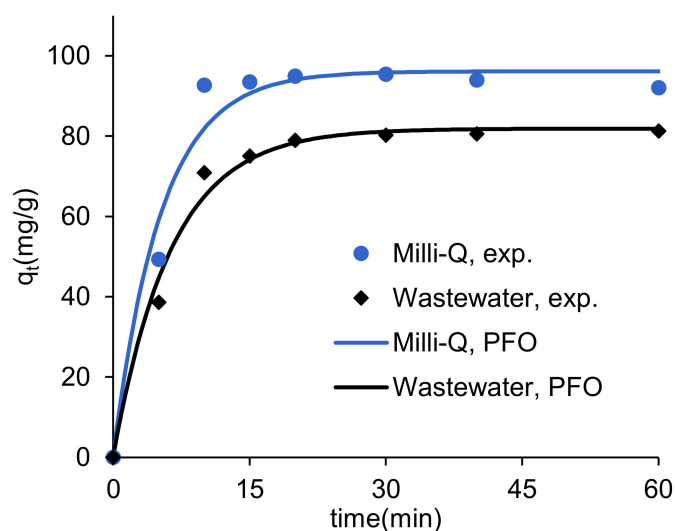


Figure 10. CPE adsorption in secondary-treated wastewater ($C_0 = 50$ mg/L, sorbent dose 0.5 g/L, initial solution pH 6.8, temperature = 22 ± 2 °C).

4. Conclusions

Despite being toxic to humans and the environment, chlorpyrifos is still a widely used pesticide in agriculture. In this study, we synthesized and characterized a novel adsorbent, γ -Fe₂O₃/Al-ZnO, and applied it for the first time to remove chlorpyrifos from both Milli-Q water and real wastewater. The adsorbent loading in γ -Fe₂O₃ of 24.52% gave the highest removal rate of CPE as compared to other higher loadings. The SEM analysis revealed the porous structure of the adsorbent, which was deemed favorable for the adsorption process, while a nitrogen isotherm at cryogenic conditions confirmed the microporous nature of the adsorbent; its BET surface area was 28.14 ± 1.48 m²/g. The interaction and effective adsorption of CPE on γ -Fe₂O₃/Al-ZnO was evidenced by EDX analysis before and after the adsorption experiments. The mechanism for CPE adsorption on γ -Fe₂O₃/Al-ZnO was suggested to proceed through interactions involving hydroxyl groups, chlorine atoms, N-pyridine, and hydrogen bonding. Following the adsorption of CPE, the magnetic property of the adsorbent was not significantly affected, making the adsorbent retrievable simply by the application of a magnetic field. The adsorption of CPE on γ -Fe₂O₃/Al-ZnO was significantly affected by pH, with the highest adsorption capacity obtained at neutral pH. The study of the CPE adsorption isotherm revealed that the Freundlich isotherm model was most suitable for describing the experimental data. In addition, the adsorption kinetics were found to be fast, with equilibrium being reached in less than 20 min, possibly due

to cooperative interactions involving the different functional groups by which adsorption takes place. The pseudo-first-order model was found to be adequate to describe the kinetic data. Considering the facile route by which γ -Fe₂O₃/Al-ZnO is synthesized, together with its efficiency in adsorption and the simplicity of retrieving it by magnetic separation, γ -Fe₂O₃/Al-ZnO could represent a versatile and promising adsorbent for the removal of emerging contaminants in water.

Author Contributions: All the authors contributed to the study design. M.B.: Investigation, Writing—original draft, Formal analysis. B.C., A.M. and A.H.: Visualization, Validation, Formal analysis, Writing—original draft. M.A.W.: Writing—review and editing. L.E.M. and A.H.H.: Investigation, Resources, Methodology, Validation. A.K. and C.T.: Methodology, Visualization, Writing—review and editing. I.T.: Methodology, Resources, Supervision, Validation, Writing—review and editing. All authors have read and agreed to the published version of the manuscript.

Funding: This research received no external funding.

Institutional Review Board Statement: Not applicable.

Data Availability Statement: The datasets presented in this study are available from the corresponding author on reasonable request.

Acknowledgments: This work is part of a doctoral thesis by Miryam Boulares. We thank the Ministry of Higher Education and Scientific Research, Tunisia, for its financial support.

Conflicts of Interest: The authors declare they have no conflict of interest.

References

1. Romero, V.; Fernandes, S.P.S.; Ková, P.; Pšenik, M.; Kolenko, Y.V.; Salonen, L.M.; Espiña, B. Efficient adsorption of endocrine-disrupting pesticides from water with a reusable magnetic covalent organic framework. *Micropor. Mesopor. Mater.* **2020**, *307*, 110523. [CrossRef]
2. NPIC. National Pesticide Information Center Snapshot, Annual Report. 2018. Available online: <http://npic.orst.edu/reports/NPIC18AR> (accessed on 27 November 2021).
3. European Union. European Commission Report of Food Safety. 2020. Available online: https://ec.europa.eu/food/plants/pesticides/approval-active-substances/renewal-approval/chlorpyrifos-chlorpyrifos-methyl_en (accessed on 9 October 2021).
4. Anwar, S.; Liaquat, F.; Khan, Q.M.; Khalid, Z.M.; Iqbal, S. Biodegradation of Chlorpyrifos and Its Hydrolysis Product 3,5,6-Trichloro-2-Pyridinol by *Bacillus Pumilus* Strain C2A1. *J. Hazard. Mater.* **2021**, *168*, 400–405. [CrossRef]
5. WHO. World Health Organization Specifications and Evaluations for Public Health Pesticides. Available online: https://www.who.int/whopes/quality/Chlorpyrifos_WHO_specs_eval_Aug_2015.pdf (accessed on 14 October 2021).
6. Mnif, W.; Hassine, A.I.H.; Bouaziz, A.; Bartegi, A.; Thomas, O.; Roig, B. Effect of Endocrine Disruptor Pesticides: A Review. *Int. J. Environ. Res. Public Health* **2011**, *8*, 2265–2303. [CrossRef]
7. IPEN. National Report on the Situation of Highly Hazardous Pesticides (HHPs), Tunisia. 2020. Available online: https://ipen.org/sites/default/files/documents/final_2july2020_tunisia_national_report_hhps.pdf (accessed on 10 September 2021).
8. Rajmohan, K.S.; Chandrasekaran, R.; Varjani, S. A Review on Occurrence of Pesticides in Environment and Current Technologies for Their Remediation and Management. *Indian J. Microbiol.* **2020**, *60*, 125–138. [CrossRef]
9. Jones, L.; Kinsella, B.; Forde, K.; Furey, A.; Regan, F. A robust analytical method for the determination of pesticide residues in wastewater. *Anal. Methods* **2017**, *9*, 4167–4174. [CrossRef]
10. Coquery, M.; Pomies, M.; Martin-Ruel, S.; Budzinski, H.; Miège, C.; Esperanza, M.; Soulier, C.; Choubert, J.-M. Measuring Micropollutants in Raw and Treated Wastewater Protocols and Results for the Analysis of Concentrations and Flows. 2011; pp. 25–43. Available online: <http://projetamperes.cemagref.fr/illustrations/25-43-COQUERY.pdf> (accessed on 8 August 2021).
11. Mejri, A.; Soriano-Molina, P.; Miralles-Cuevas, S.; Pérez, J.A.S. Fe³⁺-NTA as iron source for solar photo-Fenton at neutral pH in raceway pond reactors. *Sci. Total Environ.* **2020**, *736*, 139617. [CrossRef]
12. Soriano-Molina, P.; Plaza-Bolaños, P.; Lorenzo, A.; Agüera, A.; García Sánchez, J.L.; Malato, S.; Sánchez Pérez, J.A. Assessment of solar raceway pond reactors for removal of contaminants of emerging concern by photo-Fenton at circumneutral pH from very different municipal wastewater effluents. *Chem. Eng. J.* **2019**, *366*, 141–149. [CrossRef]
13. Wu, J.; Lan, C.; Sing Chan, G.Y. Organophosphorus Pesticide Ozonation and Formation of Oxon Intermediates. *Chemosphere* **2009**, *76*, 1308–1314. [CrossRef]
14. Zapata, A.; Oller, I.; Sirtori, C.; Rodriguez, A.; Sánchez-Pérez, J.A.; López, A.; Mezcua, M.; Malato, S. Decontamination of industrial wastewater containing pesticides by combining large-scale homogeneous solar photocatalysis and biological treatment. *Chem. Eng. J.* **2010**, *160*, 447–456. [CrossRef]
15. Saleh, I.A.; Zouari, N.; Al-Ghouti, M.A. Removal of pesticides from water and wastewater: Chemical, physical and biological treatment approaches. *Environ. Technol. Innov.* **2020**, *19*, 101026. [CrossRef]

16. Hamadeen, H.M.; Elkhatib, E.A.; Badawy, M.E.I.; Abdelgaleil, S.A.M. Green low cost nanomaterial produced from Moringa oleifera seed waste for enhanced removal of chlorpyrifos from wastewater: Mechanism and sorption studies. *J. Environ. Chem. Eng.* **2021**, *9*, 105376. [[CrossRef](#)]
17. Rafatullah, M.; Sulaiman, O.; Hashim, R.; Ahmad, A. Adsorption of copper (II), chromium (III), nickel (II) and lead (II) ions from aqueous solutions by meranti sawdust. *J. Hazard. Mater.* **2009**, *170*, 969–977. [[CrossRef](#)]
18. Zaghbani, N.; Hafiane, A.; Dhahbi, M. Removal of Safranin T from wastewater using micellar enhanced ultrafiltration. *Desalination* **2008**, *222*, 348–356. [[CrossRef](#)]
19. Jennifer, P.; Voorhees, B.M.P.; Anderson, B.S.; Tjeerdema, R.S.; Page, B. Comparison of the Relative Efficacies of Granulated Activated Carbon and Biochar to Reduce Chlorpyrifos and Imidacloprid Loading and Toxicity Using Laboratory Bench Scale Experiments. *Bull. Environ. Contam. Toxicol.* **2020**, *104*, 327–332. [[CrossRef](#)]
20. Agdi, K.; Bouaid, A.; Esteban, A.M.; Hernando, P.F.; Azmani, A.; Camara, C. Removal of atrazine and four organophosphorus pesticides from environmental waters by diatomaceous earth \pm remediation method. *J. Environ. Monit.* **2000**, *4*, 420–423. [[CrossRef](#)]
21. Ajoy Saha, V.T.G.; Gupta, S.; Kumar, R.; Ghosh, R.K. Simultaneous Removal of Pesticides from Water by Rice Husk Ash: Batch and Column Studies. *Water Environ. Res.* **2014**, *86*, 2176–2185. [[CrossRef](#)]
22. Tizaoui, C.; Fredj, S.B.; Monser, L. Polyamide-6 for the removal and recovery of the estrogenic endocrine disruptors estrone, 17 β -estradiol, 17 α -ethinylestradiol and the oxidation product 2-hydroxyestradiol in water. *Chem. Eng. J.* **2017**, *328*, 98–105. [[CrossRef](#)]
23. Mochen Liao, S.K.; Yao, Y. Generating Energy and Greenhouse Gas Inventory Data of Activated Carbon Production Using Machine Learning and Kinetic Based Process Simulation. *ACS Sustain. Chem. Eng.* **2020**, *8*, 1252–1261. [[CrossRef](#)]
24. Zahmouli, N.; Hjiri, M.; El Mir, L.; Bonavita, A.; Donato, N.; Neri, G.; Leonardi, S.G. High performance acetone sensor based on gamma-Fe₂O₃/Al-ZnO nanocomposites. *Nanotechnology* **2019**, *30*, 55502. [[CrossRef](#)]
25. Singha, D.B.; Majee, P.; Mandal, S.; Mondal, S.K.; Mahata, P. Detection of Pesticides in Aqueous Medium and in Fruit Extracts Using a Three-Dimensional Metal-Organic Framework: Experimental and Computational Study. *Inorg. Chem.* **2018**, *57*, 12155–12165. [[CrossRef](#)]
26. Manimegalai, G.; Shanthakumar, S.; Sharma, C. Silver nanoparticles: Synthesis and application in mineralization of pesticides using membrane support. *Int. Nano Lett.* **2014**, *4*, 105. [[CrossRef](#)]
27. USEPA (United States Environmental Protection Agency). Annual Report Chlorpyrifos Registration Review. Preliminary Human Health Risk Assessment; 2011. Available online: <https://www.federalregister.gov/documents/2011/07/06/2011-16729/chlorpyrifos-registration-review-preliminary-human-health-risk-assessment-notice-of-availability> (accessed on 17 September 2021).
28. Mackay, D.; Giesy, J.P.; Solomon, K.R. Fate in the Environment and Long-Range Atmospheric Transport of the Organophosphorus Insecticide, Chlorpyrifos and Its Oxon. In *Ecological Risk Assessment for Chlorpyrifos in Terrestrial and Aquatic Systems in the United States. Reviews of Environmental Contamination and Toxicology*; Giesy, J.P., Solomon, K.R., Eds.; Springer: Cham, Switzerland, 2014; Volume 231.
29. Freundlich, H. Over the adsorption in solution. *J. Phys. Chem.* **1906**, *57*, 385–470. [[CrossRef](#)]
30. Srivastava, S.; Agrawal, S.B.; Mondal, M.K. Biosorption isotherms and kinetics on removal of Cr (VI) using native and chemically modified Lagerstroemia speciosa bark. *Ecol. Eng.* **2015**, *85*, 56–66. [[CrossRef](#)]
31. Kazeminezhad, I.; Mosivand, S. Phase Transition of Electrooxidized Fe₃O₄ to gamma and alpha-Fe₂O₃ Nanoparticles Using Sintering Treatment. *Acta Phys. Pol. A* **2014**, *125*, 1210–1214. [[CrossRef](#)]
32. Sarkar, J.; Mollick, M.M.R.; Chattopadhyay, D.; Acharya, K. An eco-friendly route of γ -Fe₂O₃ nanoparticles formation and investigation of the mechanical properties of the HPMC- γ -Fe₂O₃ nanocomposites. *Bioprocess Biosyst. Eng.* **2017**, *40*, 351–359. [[CrossRef](#)]
33. Khalid, M.; Ali, A.; De la Torre, A.F.; Marrugo, K.P.; Concepcion, O.; Kamal, G.M.; Muhammad, S.; Al-Sehemi, A.G. Facile Synthesis, Spectral (IR, Mass, UV–Vis, NMR), Linear and Nonlinear Investigation of the Novel Phosphonate Compounds: A Combined Experimental and Simulation Study. *ChemistrySelect* **2020**, *5*, 2994–3006. [[CrossRef](#)]
34. Kumar, V.V.; Naresh, G.; Sudhakar, M.; Anjaneyulu, C.; Bhargava, S.K.; Tardio, J.; Reddy, V.K.; Padmasri, A.H.; Venugopal, A. An investigation on the influence of support type for Ni catalysed vapour phase hydrogenation of aqueous levulinic acid to γ -valerolactone. *RSC Adv.* **2016**, *6*, 9872–9879. [[CrossRef](#)]
35. Fu, H.; Zhou, Z.; Zhou, X. Hydrogen bonding between chlorine oxide and water (H₂O-ClO) radical complex. *Chem. Phys. Lett.* **2003**, *382*, 466–474. [[CrossRef](#)]
36. Magham, A.H.J.; Morsali, A.; Es’haghi, Z.; Beyramabadi, S.A.; Chegini, H. Density Functional Theoretical Study on the Mechanism of Adsorption of 2-Chlorophenol from Water Using γ -Fe₂O₃ Nanoparticles. *Prog. React. Kinet. Mech.* **2015**, *40*, 119–127. [[CrossRef](#)]
37. Ma, C.; Jiang, M.; Yang, C.; Yang, Z.; Meng, W.; Zhou, L.; Sun, C.; Chen, W. Construction of α -Fe₂O₃/Sulfur-Doped Polyimide Direct Z-Scheme Photocatalyst with Enhanced Solar Light Photocatalytic Activity. *ACS Omega* **2022**. [[CrossRef](#)]
38. Liu, Z.; Guo, H.; He, H.; Sun, C. Sorption and cosorption of the nonionic herbicide mefenacet and heavy metals on soil and its components. *J. Environ. Sci.* **2012**, *24*, 427–434. [[CrossRef](#)]
39. Ruthven, D.M. *Principles of Adsorption and Adsorption Processes*; John Wiley & Sons, Inc.: New York, NY, USA, 1984.
40. Hamadeen, H.M.; Elkhatib, E.A.; El Badawy, M.; Abdelgaleil, S.A.M. Novel low cost nanoparticles for enhanced removal of chlorpyrifos from wastewater: Sorption kinetics, and mechanistic studies. *Arab. J. Chem.* **2021**, *14*, 102981. [[CrossRef](#)]